Taylor dispersion analysis of metallic-based nanoparticles – A short review

Jérémie Gouyon, Ariane Boudier, Fatima Barakat, Arnaud Pallotta, Igor Clarot

Taylor dispersion analysis of metallic-based nanoparticles – a short review

Jeremie Gouyon[a]*, *Ariane Boudier*[a,b], *Fatima Barakat*[a], *Arnaud Pallotta*[a,b], *Igor Clarot*[a,b]

[a] Université de Lorraine, CITHEFOR, F-54000 Nancy, France

[b] Nanocontrol, F-54000 Nancy, France

*Correspondence should be addressed to the following author:

Jeremie Gouyon (PhD)

CITHEFOR, Université de Lorraine

F-54000 Nancy

jeremie.gouyon@univ-lorraine.fr (ORCiD number : 0000-0002-8834-9009)

Keywords: Capillary, Hydrodynamic radius, Metallic nanoparticles, Quality control, Taylor Dispersion Analysis

Abbreviations:

AgNPs	Silver nanoparticles
AuNPs	Gold nanoparticles
CRLI	Constrained Regularized Linear Inversion
d_H	Hydrodynamic diameter
DLS	Dynamic Light Scattering
FCS	Fetal Calf Serum
MUA	11-MercaptoUndecanoic Acid
NTA	Nanoparticles Tracking Analysis
PDI	Polydispersity index
PLMA	Poly(LaurylMethAcrylate)
PMA	Poly(isobutylene-alt-Maleic Anhydride)-graft-dodecyl
PTMAEMA	Poly((2-(MethAcryloyloxy)Ethyl)phosphonic Acid)
QDs	Quantum Dots
r_H	Hydrodynamic radius
SPIONs	Superparamagnetic iron oxide nanoparticles
TDA	Taylor Dispersion Analysis
ZnMCPPc	Zinc mono substituted carboxyphenoxy phthalocyanine-Glutathione-CdTe/CdS/ZnS
ZnTCPPc	Zinc tetra substituted carboxyphenoxy phthalocyanine- Glutathione - CdTe/CdS/ZnS

Abstract

Taylor Dispersion Analysis (TDA) is an interesting tool for nanoparticle (NP) size determination, feasible using simple capillary electrophoresis (CE) apparatus. Based upon the radial diffusion of analytes upon a laminar stream, the diffusion coefficient of species is easily estimable. Moreover, TDA is generally more adequate than conventional Dynamic Light Scattering (DLS) methodologies since it is less dependent on the polydispersity of the sample, leading to accurate measurement and reliable results. This review provides every paper mentioning the use of TDA for metallic-based NPs size determination. Diverse strategies for the detection of metallic NPs (like UV-Visible and inductively coupled plasma-mass spectrometry -ICP-MS- for instance) and interpretation of the Taylorgrams are discussed. Based upon the literature, advices on future prospects are also indicated, especially for comparison of TDA results with other classical techniques.

1. Introduction

Size matters when it comes to nanoparticles (NPs). To be more accurate, core size, hydrodynamic diameter (d_h, including core size and the electric dipole layer to its surface, comprising solvents and stabiliser) value and polydispersity index (PDI) strongly impact their physicochemical properties, from their bioavailability [1] to their colloidal stability [2]. For instance, cytotoxicity largely depends on the polydispersity of the NPs [3], which can be detrimental for therapeutic purposes. The use of experimental apparatus for NPs size measurement has become a critical aspect for NPs characterisation, with a wide variety of techniques available nowadays, and reviewed in the literature [4]. Transmission Electron Microscopy (TEM), NPs Tracking Analysis (NTA), Dynamic Light Scattering (DLS), UV-Visible spectroscopy, Field-Flow Fractionation, single-particle inductively coupled plasma mass spectrometry (sp-ICP-MS) or analytical ultracentrifugation are well-known examples described in various cases, from liposome [5] to ultra-small (1-3 nm range) [6] NPs characterisation. For the most popular of them, advantages and drawbacks are reported in **Table 1**, justifying the orthogonality requirements to exhaustively characterise NPs.

Table 1 - Advantages and drawbacks of the most commonly used techniques for NPs size / polydispersity determination according to the literature [7–14]

Technique	*Advantages*	*Drawbacks*
TEM	*Morphology, core size / NPs size dispersity determination shape, aggregation state*	*No information about d_h* *Large deviation for smallest size (<10 nm)* *Not representative, sample preparation and user interpretation bias* *Expensive*
DLS	*d_h determination, size distribution and dispersity, zeta potential speed and easy to use*	*Difficulties for complex media* *Sensitive to aggregates* *Bias toward larger objects in complex media* *Large deviation for smallest size (<10 nm) and for fluorescent sample* *Essential knowledge about NPs nature are required*
NTA	*d_h determination, size distribution speed and easy to use*	*Large deviation for smallest size (<10 nm)*

		Essential knowledge about NPs nature are required
TDA	***Single/double window mode**: d_h monodisperse determination* *Compatible with several detectors (UV-Visible, LIF, ICP-MS…)* *Can be considered as a separative method* *Medium viscosity determination possible*	*Experimental conditions to be controlled precisely* *Difficulties for complex media (depending on the detector)*
	***Double window mode**: counteract the influence of technical aspects (pressure ramp, injection…) on the peak variance*	*Device modification required*

NPs can be classified according to their size, polydispersity, but also their chemical composition: some are constituted of polymeric materials or macrostructural organic arrangements (such as liposomes), some will be constituted of inorganic core like mesoporous silica covered with organic moieties [15]. Others will also contain metallic or semimetallic elements, from mono-atomic complexes to metallic core in colloidal suspension. The latter – designated as metallic-based NPs – are currently gaining much attention thanks to their versatility [16]. They are tuneable (size, shape, charge) and generally characterised by surface plasmon resonance properties. They are particularly useful in bio-imaging thanks to their relative biocompatibility, and also for cancer immunotherapy in which metallic-based NPs can act as adjuvant, for instance [17]. Nowadays, metallic-based NPs and associated nanostructures are developed for a wide variety of applications, from catalysis to sensor technology [18]. Nonetheless, metallic-based NPs stability and toxicity need to be monitored, indirectly through their characterisation, including their size and PDI determination. Aforementioned size determination techniques are obviously reported in the associated literature, and the most commonly adopted. But the synthesis routes of metallic-based NPs or their use in biological media could lead to complex analytical conditions, which can be incompatible with the selected methodology. One technique can overcome some disadvantages associated to the size determination of metallic-based NPs: Taylor Dispersion Analysis (TDA). Surprisingly, TDA is almost not mentioned in the moderately recent review of S. Mourdikoudis *et al.* [4] among previously mentioned characterisation techniques. This can be explained by the low - but increasing - number

of publications dedicated to the use of TDA for NPs (20 in 2001 against 70 in 2021, see Figure 1).

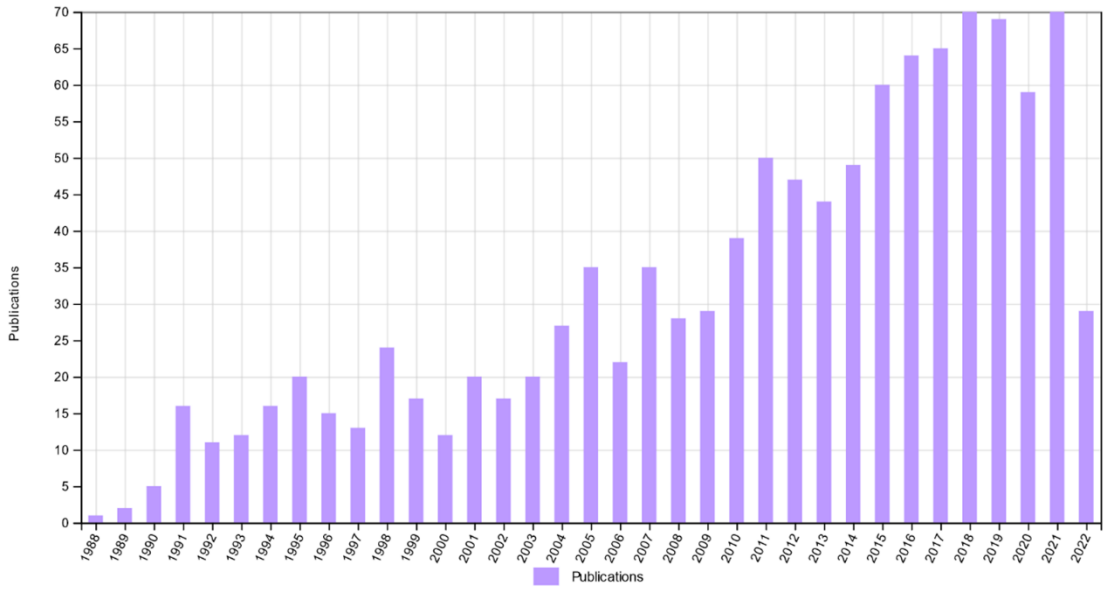

Figure 1. Number of publications related to TDA as a function of time (results obtained on WebOfScience, using "Taylor dispersion analysis" keywords for Title / Topic)

TDA is a non-destructive method adapted to d_h determination [19], ranging from Å to µm, thus including the NP range (1 to 100 nm [20]). A recent review by M.R. Moser and C.A. Baker [21], intending to bring a better comprehension of the technique and making it accessible to a wider community, gave a guide for TDA users. A particular focus was realised on practical considerations and mathematical treatment of the generated signals using pulse mode on capillary electrophoresis (CE) device, especially (originated from coupling with different detector types, such as UV-Visible or Laser induced fluorescence). Briefly, to perform TDA in pulse mode, a solute is introduced and hydrodynamically mobilised (*via* pressure difference, ΔP) through a capillary filled with a solution (buffer for example); the diffusion occurring under a laminar flow leads to a Gaussian distribution as a function of time S(t), resulting in a Taylorgram (Figure 2A) which can be fitted with equation 1 [22]:

$$S(t) = y_0 + \frac{A}{\sigma\sqrt{2\pi}}\exp\left(-\frac{1}{2}\frac{(t-t_0)^2}{\sigma^2}\right) \quad (1)$$

with t the experimental time, t_0 the mean residence time of the solute, y_0 the baseline intensity, A a constant which depends on NPs concentration and detection sensitivity,

and σ the mean temporal variance of the fitted Gaussian distribution. Using appropriate software, it is possible to approximate the signal with a theoretical curve, thus estimating σ value.

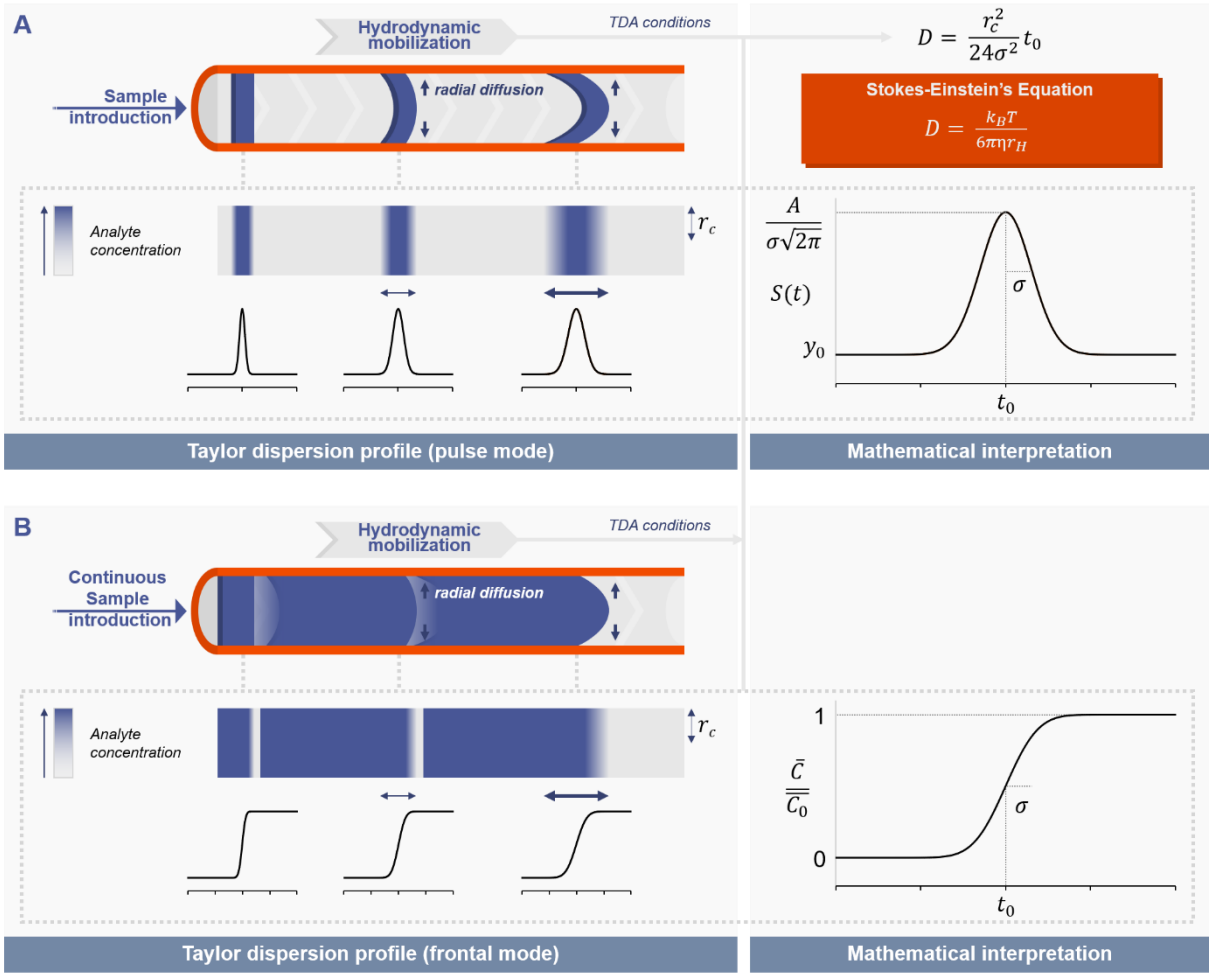

Figure 2. Principle of TDA in (A) pulse mode and Gaussian curve parameters resulting from the fitting defined in equation 1 and (B) frontal mode and frontal curve resulting from the fitting defined in equation 4. Adapted from [21]**.**

The following formula (equation 2) can be used for the determination of the diffusion coefficient of the solute D if the dimensionless residence time τ is superior to 1.4 and the Peclet number Pe is superior to 69 (defined as the 'relative rates of mass transfer along the axis of the capillary due to convection and diffusion') [23].

$D = \frac{r_c^2}{24\sigma^2} t_0$ (2), with $\tau = \frac{Dt_0}{r_c^2}$ and $Pe = \frac{ur_c}{D}$

with r_c, capillary radius and u, the linear flow rate. The previously mentioned criteria are based on previous work [23] and are generally adopted. It has been demonstrated that these conditions lead to a determination of D with a relative error ε of 1%. Then, Stokes-Einstein's equation leads to hydrodynamic radius r_h estimation (equation 3):

$$D = \frac{k_B T}{6\pi\eta r_H} \quad (3)$$

with k_B, the Boltzmann's constant, T the temperature and η the viscosity of the media inside the capillary.

In the frontal mode, the sample is continuously introduced in the capillary, leading to a Taylorgram described with a frontal curve as a function of time (Figure 2B), which can be fitted with equation 4 [23].

$$\frac{\bar{C}}{\overline{C_0}} = \frac{1}{2} \pm \frac{1}{2} erf\left[\frac{(t-t_0)}{\sigma\sqrt{2}}\right] \quad (4)$$

with $\bar{C}$ the mean solute concentration across the section of the capillary, proportional to the signal at a given time and $\overline{C_0}$ the concentration of the front, typically proportional to the signal of the front. One of the interests of the frontal mode compared to pulse mode is the lower relative standard deviation obtained for the determination of diffusion coefficient. This is attributed to a lower number of pressure changes steps, which can be detrimental toward the Taylor-Aris regime required for TDA.

In this review, we focus on the use of TDA using both modes for size determination of specific metallic-based NPs, or associated nanoobjects like nanoclusters, SuperParamagnetic Iron Oxide Nanoparticles (SPIONs) or even Quantum Dots (QDs). We aim at listing every publication mentioning the technique for such a precise application, whether it is for quality control or for deep fundamental study. Summarised in Table 2, applications, TDA conditions and main results are compared to regular characterisation techniques such as DLS or TEM, even if the considered techniques can be complementary for a wide range of NP size determination. The following paragraphs will expose the possibilities for full characterisation of NPs, in comparison with regular techniques and, regarding the reported results, advices for future development and democratisation of TDA in laboratories, for academics, industrial and regulatory purposes. TDA conditions are reported to give a quick overview of possible setups used for analysis with corresponded r_H range. The studied media are also reported since their composition affects the interactions between nanoparticles and capillary walls, which need to be negligible to remain under Taylor-Aris regime.

138 ***Table 2 – Reported application of TDA in metallic-based NPs size determination***

Application	Nanoparticle type	Ref. technique / r_H size	TDA r_H size det.	Detection technique	Studied media	TDA conditions	r_H range** (nm) *(ε=1%)*	r_H range** (nm) *(ε=3%)*	Ref.
Theoretical comparison	PVP-coated **Ag**NPs	TEM *(mean core radius)*: r_{core} = 14 ± 1,9 nm	$r_H \approx$ 23 nm	UV-Visible *(2 det.wind.)* 400 nm	MilliQ water	L_{tot} = 145 cm ; i.d. 74.5 µm ; L_{det} = 37 / 72 cm ; V_{inj} = 140 nL (2.2 %) ; ΔP = 90 mbar	[0.3 – 14.4]	[0.2 – 43.3]	[9]
	PEGylated **Au**NPs with carboxylic acid (COOH) end group	TEM *(mean core radius)*: r_{core} = 21.5 ± 4.9 nm	$r_H \approx$ 19 nm	UV-Visible *(2 det.wind.)* 520 nm					
Proof of concept for small NPs	**Au**NPs	DLS : a. r_H = - b. r_H = 13.5 ± 2 nm c. r_H = 22.5 ± 0.1 nm TEM : a. r_H = 2.3 ± 0.6 nm b. r_H = 7.5 ± 1.0 nm c. r_H = 28 ± 5 nm	a. r_H = 1.7 ± 0.1 nm b. r_H = 11.5 ± 0.5 nm c. r_H = 33.5 ± 2.0 nm	UV-Visible *(2 det.wind.)* 520 nm	0.001% (wt/V) TWEEN®20 in MilliQwater *(to prevent adsorption)*	L_{tot} = 130 cm ; i.d. 74.5 µm ; L_{det} = 45 / 85 cm ; V_{inj} = 100 - 200 nL (1.8 - 3.5 %) ; ΔP = 70 mbar	[0.4 – 20.2]	[0.3 – 60.6]	[10]
	SPIONs	DLS : a. r_H = 27 ± 1 nm b. r_H = 13.5 ± 0.2 nm TEM : a. r_{core} = 6.5 ± 1.0 nm b. r_{core} = 12.0 ± 1.5 nm	a. r_H = 7.5 ± 0.5 nm b. r_H = 16.5 ± 1.0 nm	UV-Visible *(2 det.wind.)* 280 nm					
Theoretical comparison	Citrate stabilised **SPIONs** *(2 batchs)*	TEM : a. r_{core} = 6.0 ± 0.7 nm b. r_{core} = 9.9 ± 0.6 nm	a. r_H = 6.0 ± 0.2 nm *or* 4.6 ± 0.2 nm b. r_H = 9.4 ± 0.7 nm *or* 9.3 ± 0.5 nm	UV-Visible *(2 det.wind.)* 520 nm	MilliQ water	L_{tot} = 145.5 cm ; i.d. 74.5 µm ; L_{det} = 72.5 / 104.5 cm ; V_{inj} = 112 nL (1.8 %) ; ΔP = 90 mbar	[0.4 – 28.3]	[0.2 – 85.0]	[11]
Model (related to biomedical application for spions and Au) + Industrial app. (wood impregnation Cu / pigment TiO2 / cosmetic ZnO)	Citrate stabilised **Au**NPs	TEM : r_{core} = 28,0 ± 4,7 nm	r_H = 33.8 nm	UV-Visible *(2 det.wind.)* 520 nm	MilliQwater (+0.001% (wt/V) TWEEN®20 for SPIONs / Au)	L_{tot} = 130 cm ; i.d. 74.5 µm ; L_{det} = 45 / 85 cm ; V_{inj} = - (- %) ; ΔP = 70 mbar	[0.4 – 20.2]	[0.3 – 60.6]	[13]
	SPIONs	TEM : r_{core} = 6.7 ± 1.1 nm	r_H = 7.6 nm	UV-Visible *(2 det.wind.)* 520 nm					
	ZnO-NPs	TEM : r_{core} = 28,5 ± 18.1 nm	r_H = 28.8 nm	UV-Visible *(2 det.wind.)* 280 nm					
	TiO2-NPs	TEM : r_{core} = 117.5 ± 101.4 nm	r_H = 50.0 nm	UV-Visible *(2 det.wind.)* 280 nm					
	Cu-NPs	TEM : r_{core} = 27.9 ± 26.8 nm	r_H = 33.1 nm	UV-Visible *(2 det.wind.)* 400 nm					

Theranostic agent in biological media	**Gd** chelated polysiloxane nanoparticle	DLS : r_H = 2.8 ± 0.4 nm	r_H = 2.3 ± 0.2 nm	UV 200 nm & ICP-MS	10 mM Tris + 150 mM NaCl buffer pH 7.4	L_{tot} = 70 cm ; i.d. 75 µm ; L_{det} = 21.6 cm / outlet ; V_{inj} = 8 nL (0.2 %) ; ΔP = 50 mbar	[0.3 – 7.1]	[0.2 – 21.4]	[22]
Colloïdal stability prediction	**SPIONs**	DLS : r_H = 7.3 / 9.3 / 16 nm *(sub.pop from 1 batch)*	r_H = 5.2 / 7.3 / 11.7 nm *(sub.pop from 1 batch)*	UV-Visible *(1 det.wind.) Front concentration profile* 254 nm	10 mM HCl	L_{tot} = 35 / 60 / 100 cm ; i.d. 50 µm ; L_{det} = 26.5 / 52.5 / 91.5 cm ; ΔP = 20 - 50 mbar (frontal)	[0.5 – 30.5]*	[0.3 – 91.4]*	[23]
Theoretical comparison	Highly polydisperse Citrate-capped **Ag**NPs	TEM *(no data available)*	r_H ≈ 16 nm	UV-Visible *(2 det.wind.)* 400 nm	MilliQ water	L_{tot} = 145 cm ; i.d. 74.5 µm ; L_{det} = 37 / 72 cm ; V_{inj} = 32 nL (1.0 %) ; ΔP = 90 mbar	[0.3 – 7.1]	[0.2 – 43.3]	[24]
Photodynamic therapy (nanotherapy)	Phtalocyanine conjugated **QDs** a. **Zn**TCPPc b. **Zn**MCPPc	DLS : a. r_H = 13.6 ± 7.0 b. r_H = 67.1 ± 32.9 nm	a. r_H = 13.5 ± 3.9 nm b. r_H = 64.1 ± 7.7 nm	IF/UV-Visible *(2 det.wind.) Front concentration profile* 480 nm ex. / 630 nm em. / 680 nm abs.	phosphate buffer pH 7.4 I.S. 15 mM *(and other media)*	L_{tot} = 45 cm ; i.d. 50 µm ; L_{det} = 21 (IF) / 36.5 (UV) cm ; ΔP = 70 mbar	[1.2 – 37.5] (IF) / [1.2 – 65.3] (UV)	[0.7 – 112.6] (IF) / [0.7 – 195.8] (UV)	[25]
Colloïdal stability prediction	Hydrophilic surface coated **Au**NPs a. PMA-**Au**NPs b. PEG-2kDa-PMA-**Au**NPs c. PEG-10kDa-PMA-**Au**NPs d. MUA-**Au**NPs e. PTMAEMA-stat-PLMA-**Au**NPs PEG-10kDa-PMA-**Au**NPs MUA-**Au**NPs PTMAEMA-stat-PLMA-**Au**NPs	DLS *(cumulant method)* a. r_H = 26.80 ± 0.09 nm b. r_H = 22.46 ± 0.11 nm c. r_H = 33.74 ± 0.14 nm d. r_H = 19.59 ± 0.09 nm e. r_H = 11.15 ± 0.14 nm	a. r_H = 9.22 ± 0.10 nm b. r_H = 12.81 ± 0.13 nm c. r_H = 14.44 ± 0.19 nm d. r_H = 8.08 ± 0.08 nm e. r_H = 5.98 ± 0.04 nm	UV-Visible *(1 det.wind.) Front concentration profile* 280 nm	5 mM disodiumtetraborate decahydrate	L_{tot} = 61.5 cm ; i.d. 75 µm ; L_{det} = 51.4 cm ; V_{inj} = 24 nL (0.9 %) ; ΔP = 70 mbar	[1.0– 53.9]	[0.6 – 161.8]	[14,26]
Cancer diagnosis and therapy	Carboxylic-acid modified fluorescently labelled **SPIONs** silica core-shell (NP*-COOH): a. (NP*-COOH) *without aptamer* b . NP*-COOH *with aptamer 1/150*	DLS : a. r_H = 32 nm b. - c. -	a. r_H = 34.5 ± 2.5 nm b. r_H = 39.5 nm c. r_H = 41.5 nm	UV-Visible *(1 det.wind.) Front concentration profile* 254 nm	MOPS buffer pH 7.4 I.S. 100 mM	L_{tot} = 35 cm ; i.d. 50 µm ; L_{det} = 26.5 cm ; ΔP = 50 mbar (frontal)	[0.5 – 30.5]	[0.3 – 91.4]	[27]

	c. NP*-COOH *with aptamer 1/200*								
Nanoparticle-based biocataclyst	**Au**NPs a. Citrate stabilised **Au**NPs b. Pepsin-**Au**NPs* **other pepsin concentration were tested*	DLS : a. r_H = 22.1 ± 0.2 nm b. r_H = 39.9 ± 2.9 nm TEM : a. r_{core} ≈ 15 nm b. -	a. r_H = 17.8 ± 0.2 nm b. r_H = 21.5 ± 0.3 nm	UV-Visible *(2 det.wind.)* 214 nm	Ultrapure water	L_{tot} = 130 cm ; i.d. 75 µm ; L_{det} = 44 / 85 cm ; V_{inj} = 40 nL (0.7 %) ; ΔP = 140 mbar	[0.2 – 9.6	[0.1 – 28.9]	[28]
Effective charge determination	Carboxylated magnetic beads *(commercial **SPIONs**)*	-	r_H = 100 ± 0.15 nm (given by the manufacturer)	UV-Visible *(1 det.wind.)* 200 nm	Water	L_{tot} = 33.5 cm ; i.d. 50 µm ; L_{det} = 25 cm ; V_{inj} = 2.6 nL (0.4 %) ; ΔP = 50 mbar	[0.5 – 20.0]	[0.3 – 59.9]	[29]
	CeO_2	-	r_H = 16.05 ± 0.48 nm	UV-Visible *(1 det.wind.)* 254 nm	Betaine-Cl^- pH 2 I.S. 10 mM				
	TiO_2	-	r_H = 13.71 ± 0.55 nm	UV-Visible *(1 det.wind.)* 254 nm	Betaine-Cl^- pH 2 I.S. 10 mM				
Gd speciation	**AGuIX** ultrasmall nanoparticles (gadolinium-chelated polysiloxane nano-Particles)	-	r_H = 2.8 ± 0.1 nm *(bimodal deconvolution)* r_H = 2.7 ± 0.1 nm *(CRLI)*	ICP-MS	10 mM Tris + 150 mM NaCl buffer pH 7.4	L_{tot} = 70 cm ; i.d. 75 µm ; L_{det} = outlet ; V_{inj} = 7 nL (0.2 %) ; ΔP = 50 mbar	[0.3 – 23.1]	[0.2 – 69.2]	[30]
Protein corona formation on Au-Si-NPs	**Au**SiNPs a. protein-free b. with BSA c. with fetuin from FET	DLS : a. r_H = 30 ± 2 nm TEM : a. r_{core} = 28.5 ± 1.5 nm	a. r_H = 30.0 ± 0.7 nm b. r_H = 36.8 ± 0.7 nm c. r_H = 35 ± 1 nm	ICP-MS	10 mM phosphate buffer pH 7.4	L_{tot} = 70 cm ; i.d. 50 µm ; L_{det} = outlet ; V_{inj} = 2.9 nL (0.2 %) ; ΔP = 50 mbar	[1.1 – 116.8]	[0.6 – 350.5]	[31]

Note : PVP = PolyVinylPyrrolidone ; PMA = Poly(isobutylene-alt-Maleic Anhydride)-graft-dodecyl ; MUA = 11-MercaptoUndecanoic Acid ; PTMAEMA = Poly((2-(MethAcryloyloxy)Ethyl)phosphonic Acid) ; PLMA = Poly(LaurylMethAcrylate); NP = fluorescently labelled NPs ; I.S. = Ionic Strenght*
Different samples in the same article are identified by letters (a, b, c…)
** estimated by considering L_{tot} = 35 cm, L_{det} = 26.5 cm ;* ΔP = 50 mbar
**r_H range are estimated using TDA conditions as described in the corresponding paper and : for ε = 1%, Pe > 69 and τ > 1.4 and for ε = 3%, Pe > 40 and τ > 1.2 using equations 2 and 3

139

2. Capillary device for TDA applications

2.1. Single window mode

Capillary Electrophoresis is a separative technique based upon the application of an electric field in a capillary filled with electrolyte buffer. Due to the reduced inner capillary diameter (down to 5 µm) and pumping system adapted to relatively low laminar flow control, CE apparatus is well-suited for TDA, even though some other devices can be used as it will be presented. Previously mentioned criteria on τ and Pe values can be easily satisfied according to the analyte size and capillary dimensions (such as capillary length or inner diameter) for both pulse and frontal mode. Another advantage of CE is the inline coupling with UV-Visible detector, making it easy to monitor most of the NPs since they generally possess optical properties, from deep UV to visible absorbance range (Figure 3A).

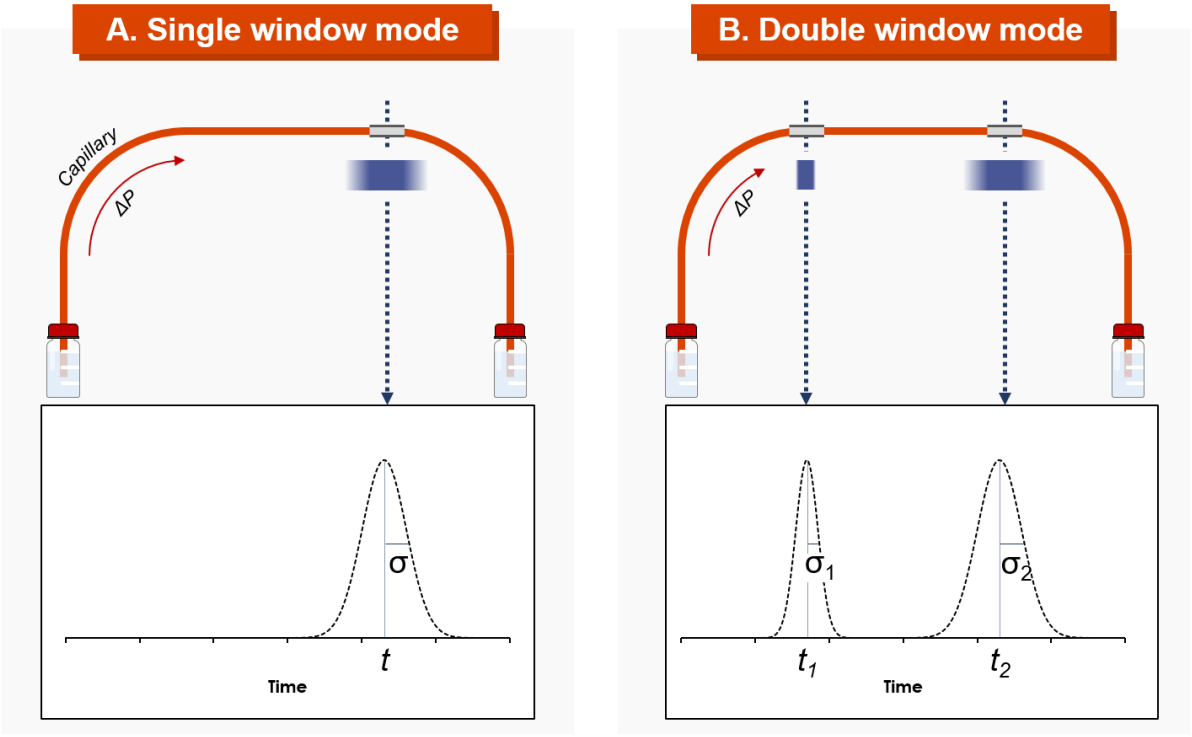

Figure 3. Scheme of TDA with CE device in (A) single window mode and (B) double window mode.

Historically, the first use of CE for TDA application was reported in 1994 by M.S. Bello *et al.* [32], with a proof of concept based on the determination of the diffusion coefficient of small organic molecules and proteins. A single UV-Visible detector was used inline and the results were in good agreement with the tabulated values of the literature. The technique has been presented as an accessible tool for bioanalytical laboratories since relatively regular devices are required (compared to DLS devices, back at the time) but

also for a quick determination and a low sample consumption, which is quite advantageous when analysing biological samples. It was only in 2008 that the first use of CE device for TDA of metallic-based NPs was reported, with the characterisation of Maghemite particles (or SPIONs) in a single window mode (also denoted as single-point detection configuration) [23]. Careful considerations were taken using TDA as described in other papers, such as the effect of a flow ramp while mobilising the fluid through the capillary [33], or an absence of interaction between the particles and the capillary inner wall [34]. Didodecyldimethylammonium bromide was used as dynamic coating reagent between each run to limit particle–capillary inner wall interactions and size-exclusion effect (SPIONS being cationic and uncoated silica capillary being anionic at neutral pH), ensuring that the mean axial velocity of the NPs is equivalent to that of the electrolyte.

Performing TDA in hydrochloric acid (HCl) background electrolyte (BGE) from a front concentration profile (using frontal mode) on three sorted size populations (below 10 nm diameter), F. d'Orlyé *et al.* [23] successfully determined the SPIONs d_H, comprised between 10.4 and 23.4 nm (Table 2). It is noteworthy that TDA results tend to be superior to particle mean solid radii estimated by magnetic measurements, attributed to hydration effects.

They also pointed out DLS results for comparison, with overestimated r_H of around 30%, which is inherent to the technique. Indeed, DLS intensity is proportional to the square of the particle volume/mass, implying that the largest particles will strongly impact the results and potentially lead to an overestimation of the real NPs size (Figure 4). Since TDA is measured with a UV-Visible detector, the signal is proportional to the mass concentration, which is less impacted by the polydispersity, unlike DLS measurements. The main interest of this study was to examine colloidal stability through estimation of the diffusion coefficient, discerning interaction and aggregation phenomena, while limiting the impact of partial aggregation on the size determination. Showing the existence of repulsive interactions between SPIONs, the influence of electrolyte ionic strength has been highlighted. Addition of sodium chloride to the BGE to tune ionic strength allowed to decrease NPs interactions, which accounted for the determination of the Brownian diffusion coefficient of a single sphere. Thus, BGE composition is of utmost importance in the determination of NPs size since D is dependent on NPs interactions.

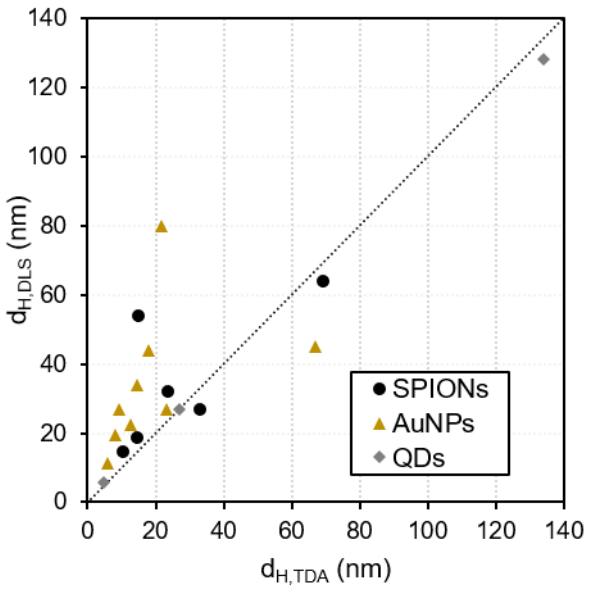

Figure 4. DLS hydrodynamic diameter as a function of the TDA measurements reported from various papers ; some NPs may be constituted of aggregates [10,22,23,25–28]**. $d_{H,DLS}$ and $d_{H,TDA}$ refer to d_H measured by DLS and TDA, respectively.**

The same team used a similar strategy to characterise silica core-shell SPIONs, chemically modified with an aptamer for miniaturised molecular diagnostic tool development [27]. Since silica core shell SPIONs were doomed to be characterised by Capillary Zone Electrophoresis (CZE) separation, TDA was naturally chosen to complete NPs characterisation. They demonstrated that associated devices are helpful in the development of biocompatible tools, with determination of the grafting efficiency and prediction of the conditions in which SPIONs will aggregate. They evidenced the successful grafting of synthetic oligonucleotides on maghemite, with an evolution of d_h from 69 nm to up to 83 nm, with a colloidal suspension and no apparent aggregation. In this case, both DLS and TDA gave close results, which can be attributed to a low PDI (less than 0.1 before grafting). No additional details were given about experimental conditions, except the use of a BGE composed of 3-(N-morpholino)propanesulfonic acid (MOPS) buffer (I.S. = 100 mM, pH 7.4). A near-neutral pH was selected since CZE measurements were shorter, and insuring no aggregation for both SPIONs and aptamer grafted SPIONs.

In a more anecdotal way, TDA coupled with UV-visible detection was also used for inorganic NPs size estimation such as CeO_2 and TiO_2 [29], but sizes were not compared to any other regular technique; it testifies the confidence of the team,

working actively with TDA for the determination of d_H (see Table 2 for reference [29]), on the development of TDA for the analysis of mixtures for instance [35]. Analyses were performed in an acidic BGE (betaine/chloride pH 2) to prevent CeO_2 and TiO_2 precipitation, but also for further CZE experiments.

In the same manner, U. Pyell *et al.* [14,26] used TDA to characterise five different gold NPs (AuNPs), with a negatively charged surface obtained after coating with amphiphilic polymer or polyethyleneglycol (PEG). Since interactions between NPs and inner wall of the capillary are detrimental for TDA and CZE experiments, an alkaline aqueous BGE (pH ~ 9) was chosen (5 mM borate buffer) to yield a negatively charged inner capillary surface, since AuNPs were negatively charged and thus suppressing potential interactions. With AuNPs of hydrodynamic radii determined by TDA ($r_{H,TDA}$) ranging from 5.98 to 15.44 nm, (for Au-core of about 2 nm), they confronted those results with DLS measurements. Actually, they did compare TDA appreciation with the number-weighted means hydrodynamic radii ($r_{H,DLS,N}$) obtained by employing the CONTIN algorithm on the DLS acquisition [36] for interpretation. It is important to highlight that depending on the DLS size characterising parameters used for comparison with $r_{H,TDA}$, there could be an important deviation. Careful attention should be paid to the exact DLS size characterising parameters and mathematical approach reported in the literature, which is not systematically indicated in experimental papers according to our reading (Figure 5).

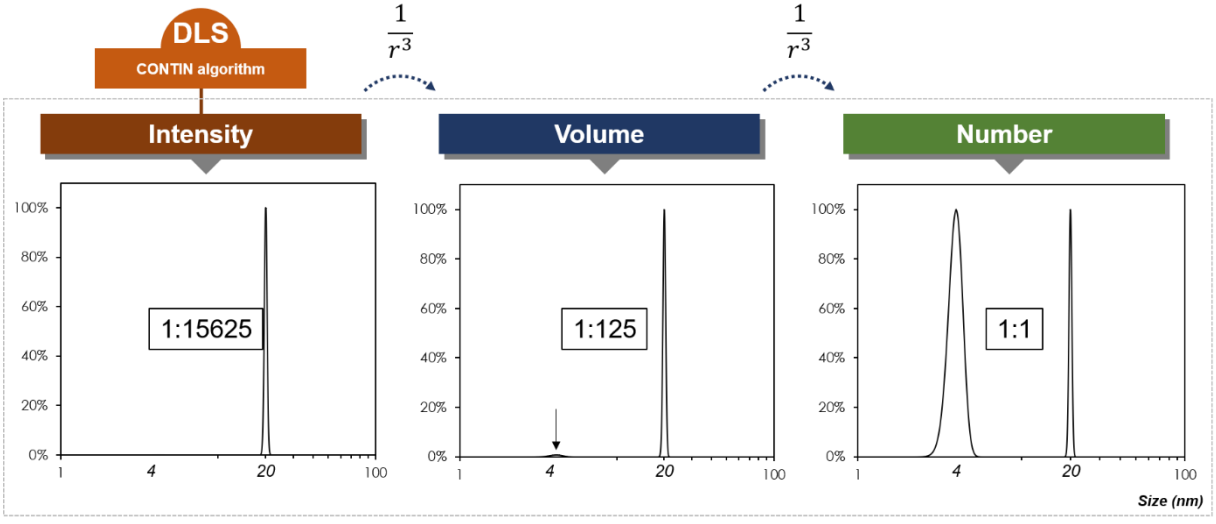

Figure 5. DLS treatment types and graphical representation of intensity, volume and number distribution. DLS acquisitions are first treated with the CONTIN algorithm, which results in intensity distribution graphic. Since DLS signals are proportional to the NPs radius power of 6, the conversion in volume distribution

is done by dividing to radius to power of 3, while number distribution approximation is divided by the radius to the power of 6, resulting in variable radius value when comparing the different distribution. One may consider each data when reporting r_H values, or should at least indicates the distribution type used in the report. In this example, 2 subpopulations of 4.0 and 20.0 nm respectively (σ = 0.4 nm for each population) are represented with an initial ratio of 1:15625 in intensity distribution. Since there is a ratio 1:5 between both NPs size, the volume distribution gives a ratio 1:(15625/5^3) = 1:125, and 1:(15625/5^6) = 1:1 for number distribution. Mean radius values in this representation are equal to 20.1 ± 0,4, 19.9 ± 1,5 and 12.0 ± 8,0 nm for each distribution, respectively, which justifies the requirement of DLS information, when reported in the literature.

For instance, CONTIN algorithm is well suited for polydisperse sample analysis, while the cumulant method is generally commonly adopted for monomodal population. As concluded by U. Pyell *et al.* [14,26], using CE device coupled with a UV detector, TDA allows the estimation of number-weighted and volume-weighted mean hydrodynamic radii.

Moreover, TDA evidenced a subpopulation for two different AuNPs, possibly attributed to agglomerates as highlighted with DLS $r_{H,N}$ estimation (Table 2, for references [14,26]). This was demonstrated by a deviation of the fitting curve (based on a Gaussian cumulative function, using pulse mode) from the experimental Taylorgram, which is interpreted here by the presence of larger AuNPs in the media.

Finally, G. Ramírez-García *et al.* worked on the characterisation of functionalised QDs, using TDA to measure the apparent equivalent sphere diameter of the metallic-based NPs, with coupling to either UV-Visible and/or fluorescence detectors [25]. Frontal mode was used with adequate equations from previously mentioned paper [23], with mathematical models being very well-fitted to the Taylorgram. Size but also surface charge and stability of the QDs were concomitantly estimated by CZE, with a particular interest to the comparison between TDA and DLS results. No interaction between the capillary and the NPs was highlighted, since no variation of the retention time occurred. QDs consisted of zinc mono substituted carboxyphenoxy phthalocyanine-Glutathione-CdTe/CdS/ZnS (ZnMCPPc-QDs) and zinc tetra substituted carboxyphenoxy phthalocyanine- Glutathione -CdTe/CdS/ZnS (ZnTCPPc-QDs). The colloidal stability of ZnTCPPc-QDs in low ionic strength was evidenced since TDA measurements

indicated a d_H of around 27 nm, while ZnMCPPc-QDs was measured at around 130 nm. This was explained by the presence of aggregates due to lower electrostatic repulsions since the latter contains only one carboxyl group. In this case, TDA gave lower standard deviation value than DLS, since QDs aggregates strongly impact the latter, but also since alteration of the refractive index is due to the fluorescence properties of the NPs and by the incident laser light absorption (Table 2, for reference [25]). In this situation, TDA with CE apparatus clearly presents the advantage of filling the inherent inconveniences originated from the DLS methodology, while working in physiologically relevant condition.

Another interesting coupling with TDA is the use of ICP-MS as detector in order to increase the specificity since UV-Visible detector or DLS measurements are sensitive to matrix interferences. Single particle ICP-MS can be used to determine metallic content of a suspension [37], allowing analysis in complex media. This methodology can be used alone to determine NP size, but is not adapted to hybrid NPs (composed of multiple metals) since intensity of the signal depends on the metallic composition. Coupling of ICP-MS with TDA allows to characterise a wider range of sizes and compositions of NPs. Experimental conditions were assessed using previous work of H. Cottet's team [38,39], in which they expressed a range of operating mobilising pressure based upon a relative error on the determination of D of 3% instead of 1% (translated here by following prerequisite : Pe > 40 and $\tau > 1.2$). Using a gadolinium-containing theragnostic NP for TDA coupled with ICP-MS, L. Labied *et al.* [22] measured a hydrodynamic radius of 2.2 nm in pulse mode, accurate with DLS measurements. They also highlighted the existence of a slight polydispersity since Taylorgrams presented slight deviation from the Gaussian fitting model. One of the advantages of using ICP-MS with TDA instead of DLS is the lower concentration of sample required for proper detection (down to 0.05 $g.L^{-1}$, 200 times lower), but also the multi-elemental character of the detector, allowing for multiplex assay. The same team also worked on the size determination of a commercially available gadolinium-chelated polysiloxane NPs (AGuIX) [30], using a bimodal fitting in comparison with a constrained regularised linear inversion (CRLI) method. They were able to discriminate two subpopulations with only few nanometers differences, one comprising Gadolinium-containing ultrasmall NPs (5.4 ± 0.2 nm), and a second comprising its fragments (1.8 ± 1.6 nm), which is hardly feasible with DLS.

They also worked on the protein corona formation on gold silica NPs (AuSiNPs) [31], arguing that ICP-MS allows to detect metallic content selectively in complex biological media. Studying the adsorption of proteins (bovine serum albumin, BSA and fetuin from fetal calf serum, FCS), the team showed the formation of protein layers on the surface of the AuSiNPs (r_H = 30.0 ± 0.7 nm) with an increase to up to 36.8 ± 0.7 nm (12.5 $mg_{BSA}.mL^{-1}$) and 35 ± 1 nm (15 $mg_{FCS}.mL^{-1}$) respectively. The change in r_H suggests the formation of a protein monolayer in the described conditions. In the case of FCS incubation, higher concentrations were tested (up to 30 $mg_{FCS}.mL^{-1}$), resulting in probable NPs aggregation of protein multilayer. The reversibility of the protein corona formation was also studied, showing that BSA corona stability is influenced by incubation time of AuSiNPs with the protein, with a reversible corona, if incubation time is too short (2 h). For longer incubation time tested in the study (4 h), an irreversible corona was evidenced through TDA measurements, explained since irreversible adsorption of BSA requires structural changes in the adsorbed BSA, occurring for longer incubation time. In the case of fetuin corona, a hard corona was evidenced with the formation of a monolayer upon the surface of the NPs, and that NPs or protein aggregation occurring in concentrated protein-containing media are reversible.

As mentioned in this paragraph, one of the main applications of TDA in single window mode remains in the size estimation but also in the determination of the colloidal stability, with the advantage of being more precise than DLS. Another advantage is that the use of CE apparatus is generally concomitant to CZE analysis, which allows charge determination through measurement of the electrophoretic mobility [29], while working with low sample volume. Coupling with ICP-MS allows better selectivity towards metals constituting the NPs, which has been presented as an interesting mode for study in complex media.

2.2. Double window mode

To counteract the influence of the injected volume and pressure ramp on the peak variance and elution time, a two-detection window mode (also denoted as dual-point detection configuration, Figure 3B) was first proposed by A.J.S. Chapman and D.M. Goodall [40]. It consists in using two detection points during the same analysis to highlight the influences of the analytical running conditions on the results. J. Chamieh *et al.* [41,42] demonstrated that for low injection volume (< 1% capillary volume till the detection window), there is no significant difference between d_H estimated with a

single-window and a double-window approach. Still, the use of the latter is preferable since there is no need for approximation, and it increases the sensitivity of the detector (with higher injected volume for instance), at least for monodisperse NPs. The conception of a double window apparatus is not simple, which is why it is not systematically used for TDA. It requires changes of the regular apparatus, with in-house development adaptation, even if several strategies have been presented in the literature as illustrated in the following section. In the case of double-window mode, the Taylor-Aris equation is modified as follows (equation 5):

$$D = \frac{r_c^2}{24(\sigma_2{}^2 - \sigma_1{}^2)}(t_2 - t_1) \quad (5)$$

with t_1 and t_2 the mean residence time of the solute to reach the first and second window respectively, and σ_1 and σ_2 the mean temporal variance of the fitted Gaussian distribution at the first and second window respectively, as illustrated in Figure 3B.

One use of this technique for AuNPs characterisation has been presented by M. Höldrich *et al.* [28], with analysis of pepsin-coated AuNPs to study the mechanism of formation of protein corona, as potential use for nanobiocatalyst with attachment of enzyme on metallic NPs. In this study, TDA was employed on a Viscosizer device since DLS results were questionable, due to the sensitivity of the method towards bigger NPs, responsible for probable particle distribution distortion. This can lead to undistinguishable r_H between pepsin-coated AuNPs at different pepsin incubation concentration. It has to be noted that TDA conditions were not discussed, especially concerning the boundary conditions in which TDA is applicable (τ and Pe). Results showed that TDA was useful and sufficiently resolved to distinguish uncoated AuNPs (citrate-capped, r_H = 17.8 ± 0.2 nm) and pepsin-coated AuNPs (up to 21.5 ± 0.3 nm), in agreement with DLS results and allowing to distinguish r_H for different pepsin concentration level incubating with AuNPs. It is noteworthy that when analysing citrate-capped AuNPs, Taylorgrams with peaks corresponding to a bimodal distribution were evidenced. Deconvolution of the signal were done with two overlapping Gaussian signals, one attributed to free citrate in solution and another to citrate-capped AuNPs. Pepsin grafting occurs through ligand exchange mechanism by monolayer formation. The binding isotherm built from r_H of AuNPs as a function of the logarithm of the pepsin concentration led to an effective dissociation constant of 30.7 µM. Data from TDA measurements were used for estimation of the amount of bound pepsin, in the same

order with the one determined by Lowry's assay for an intermediate studied pepsin concentration incubation (1 mg/mL, 89200 against 51745 pepsin/AuNPs respectively). The dual detection window mode has been extensively used by S. Balog *et al.* [9–11,13,24] for several applications in metallic-based NPs, from AuNPs to SPIONs TDA characterisation with a particular interest in theoretical predictions for a better modelling to estimation of d_H, especially concerning polydisperse samples.

A first study aimed at comparing TDA results for the characterisation of diverse NPs with sizes obtained by DLS and TEM [10]. Citrate-capped AuNPs (d_H between 3.3 and 67 nm TDA) and SPIONs (d_H between 15 and 33 nm TDA) showed higher results than TEM measurements in most cases (except for lower sizes of AuNPs). This is attributed to the fact that TDA is used for d_H determination, TEM resulting in a core-dried state which implies a lower value than in aqueous media. Deviation from DLS, however, was attributed to the presence of larger NPs and/or aggregates, as discussed previously in this paper. This tends to be overestimated when using light scattering and justifies the use of TDA instead of DLS. It has to be pointed out that authors highlighted the determination of two different sizes with DLS, one based on cumulant analysis, another on CONTIN analysis [43]. Careful attention was already given to the reader to interpret these characteristics. Another important note is that the lower tested sizes (for AuNPs) gave results with TDA in good agreement with TEM, in contrary to DLS which tends to be problematic when NPs became too small (below 2 nm here). So TDA can be used for small size determination with low sample consumption, oppositely to DLS.

A second study [13] aimed at developing a new model describing the polydispersity affecting the Taylorgram in pulse mode, which results in a non-Gaussian curve since it consists in an overlay of multiple Gaussian curves. By considering the size-dependent optical extinction $\mu(r, \lambda)$ of a particle at the detection wavelength, they introduced the probability density distribution of the particle radius in the Taylorgram expression, P(r). To illustrate their model, two metallic-based NPs were tested and accurately measured by considering that optical extinction is dominated by absorption. Citrate-capped AuNPs and SPIONs apparent radii were measured at 33.8 nm and 7.6 nm experimentally, against 30.4 nm and 7.2 nm predicted with TEM results, respectively (Table 2). This tends to demonstrate the validity of the methodology and the equations used to describe the results. Industrial samples of ZnO, TiO_2 and Cu NPs were also tested according to the same process, resulting in non-Gaussian Taylorgrams and/or multimodal and asymmetric distribution. Large polydispersities

were expected for the samples, which were testified by TEM measurements. But due to low signal-to-noise ratio, TDA cannot provide clear information about population fraction resulting from aggregates and agglomerates. In the case of CuNPs, matrix interferences (molecules or subnanometer particulates) were also responsible for overlapping a narrow peak to the Taylorgram, but were not further discussed.

A third study focused on the possibility to improve the dynamic range of TDA [11]; actually, proper particle size determination with TDA is operational with only a valid combination of parameters, comprising capillary inner diameter size, mobilisation pressure, injected volume and so on. This can be particularly tricky when working with weakly absorbing colloids (UV-Visible), but also for routine analysis when comparing different NPs sizes. To counteract this inconvenient and to extend the use of TDA for a wide dynamic range for a given apparatus, P. Lemal *et al.* considered TDA as a linear time-invariant system [11]. A new equation describing the signal, suited either for mono or moderately polydisperse NPs, has been proposed and used for SPIONs characterisation with sample volume of around 1.8 % of the total capillary volume. TDA results gave better estimation on the basis of the linear time-invariant system with 6.0 ± 0.2 nm against 4.8 ± 0.2 nm with regular consideration, for 6.0 ± 0.7 nm determined with TEM. Larger NPs were correctly estimated with both models (9.4 ± 0.7 nm and 9.3 ± 0.5 nm for linear time-invariant system and regular consideration respectfully against 9.9 ± 0.6 nm with TEM), highlighting particle size impact on the accuracy of the method. The development of a new equation for the description of the Taylorgram was needed to extend the dynamic range of size estimation while using a single set of parameters. As written, “for a given range of particle sizes, one may always find a valid combination of operation parameters”, which is not always compatible with routine analysis or for the uninitiated. The new equation allows for the determination of uniform and moderately polydisperse particles with arbitrary injection and detection volumes, which is interesting for an increase in sensitivity towards NPs with low absorbance properties.

Using similar approach, P. Taladriz-Blanco *et al.* [9] described, with a mathematical model, the Taylorgram originating from polymer coated AuNPs and AgNPs, with good accuracy between theoretical approach and experimental results. TDA gave sizes reported in Table 2 (around 20 nm each), but were not discussed since it was not the purpose of the paper. However, higher values were obtained with TDA approach than

TEM results, which is in good agreement with previously reported remarks on similar metallic NPs.

Finally, the team worked on another mathematical model, reliable for highly polydisperse AgNPs suspension [24] and describing the limit of resolution of TDA. Actually, resolution of TDA was explored, *i.e.* the capacity to resolve the difference between r_H and $r_H \pm \delta_r$. Temperature, viscosity, capillary radius or peak width were identified as directly related to the "precision" of the measurement. The regular model was used to estimate AgNPs size (around 16 nm), using TEM to validate the high polydispersity of the sample (no data available). The main interest of the study was not only to present the analysis of a degradable metallic NPs as a function of time (with evolution of the r_H as a function of time). It was also to use a new mathematical description of the polydispersity, with good agreement with the prediction. However, the low signal-to-noise ratio did not allow for high resolution, owing to differentiate particle size and comparing experimental results and theoretical expectation with good accuracy.

3. Conclusion

TDA has been proven as a promising characterisation tool for metallic-based NPs size determination, and easily implementable in laboratories since CE apparatus are perfectly equipped for this application. UV detector in single or double window mode have been extensively used for various metallic-based NPs characterisation (Au, Ag, Fe, …). Other couplings are still being optimised. ICP-MS, for instance, allows for a better specificity toward metals, reducing the interferences due to matrix component, promising for complex media study such as for protein corona formation. CZE coupling is also feasible, and coherent since no significant modification of the CE apparatus is required.

TDA allows for the determination of monodisperse NPs population, since signals originated from NPs are directly proportional to the mass of the metal. In the case of polydisperse NPs, theoretical studies are still in progress, with mathematical approximations requiring a sensitive detection method to increase the resolution and thus the exact PDI of a sample. Nonetheless, numerous teams are nowadays using TDA in both pulse and frontal mode as a potential routine tool and are confident enough to conclude about NPs size using only this methodology. Using both single and double window mode (the latter being less accessible since it requires customisable device),

metallic-based NPs size has been screened from sub-NPs to larger inorganic objects (r_H ranging from 2.3 to 128.2 nm), making it a suitable alternative to DLS measurements.

Conflict of interest

The authors have declared no conflict of interest.

Author contributions

Conceptualisation, J.G., I.C. and A.B.; writing—original draft preparation, J.G.; writing—review and editing, J.G., A.B., F.B., A.P. and I.C. All authors have read and agreed to the published version of the manuscript.

Data Availability Statement

Data sharing not applicable to this article as no datasets were generated or analysed during the current study.

4. References

[1] Zarschler K, Rocks L, Licciardello N, Boselli L, Polo E, Garcia KP, et al. Ultrasmall inorganic nanoparticles: State-of-the-art and perspectives for biomedical applications. Nanomedicine Nanotechnol Biol Med 2016;12:1663–701.

[2] Pyell U, Jalil AH, Pfeiffer C, Pelaz B, Parak WJ. Characterization of gold nanoparticles with different hydrophilic coatings via capillary electrophoresis and Taylor dispersion analysis. Part I: Determination of the zeta potential employing a modified analytic approximation. J Colloid Interface Sci 2015;450:288–300.

[3] Pan Y, Neuss S, Leifert A, Fischler M, Wen F, Simon U, et al. Size-dependent cytotoxicity of gold nanoparticles. Small Weinh Bergstr Ger 2007;3:1941–9.

[4] Mourdikoudis S, Pallares RM, Thanh NTK. Characterization techniques for nanoparticles: comparison and complementarity upon studying nanoparticle properties. Nanoscale 2018;10:12871–934.

[5] Fan Y, Marioli M, Zhang K. Analytical characterization of liposomes and other lipid nanoparticles for drug delivery. J Pharm Biomed Anal 2021;192:113642.

[6] Kim BH, Hackett MJ, Park J, Hyeon T. Synthesis, Characterization, and Application of Ultrasmall Nanoparticles. Chem Mater 2014;26:59–71.

[7] Chetwynd AJ, Guggenheim EJ, Briffa SM, Thorn JA, Lynch I, Valsami-Jones E. Current Application of Capillary Electrophoresis in Nanomaterial Characterisation and Its Potential to Characterise the Protein and Small Molecule Corona. Nanomaterials 2018;8:99.

[8] Deleanu M, Hernandez J-F, Cipelletti L, Biron J-P, Rossi E, Taverna M, et al. Unraveling the Speciation of β-Amyloid Peptides during the Aggregation Process by Taylor Dispersion Analysis. Anal Chem 2021;93:6523–33.

[9] Taladriz-Blanco P, Rothen-Rutishauser B, Petri-Fink A, Balog S. Versatile Macroscale Concentration Gradients of Nanoparticles in Soft Nanocomposites. Small 2020;16:1905192.

[10] Urban DA, Milosevic AM, Bossert D, Crippa F, Moore TL, Geers C, et al. Taylor Dispersion of Inorganic Nanoparticles and Comparison to Dynamic Light

Scattering and Transmission Electron Microscopy. Colloid Interface Sci Commun 2018;22:29–33.
[11] Lemal P, Petri-Fink A, Balog S. Nanoparticles and Taylor Dispersion as a Linear Time-Invariant System. Anal Chem 2019;91:1217–21.
[12] Balog S. Taylor Dispersion of Polydisperse Nanoclusters and Nanoparticles: Modeling, Simulation, and Analysis. Anal Chem 2018;90:4258–62.
[13] Balog S, Urban DA, Milosevic AM, Crippa F, Rothen-Rutishauser B, Petri-Fink A. Taylor dispersion of nanoparticles. J Nanoparticle Res 2017;19:287.
[14] Pyell U, Jalil AH, Urban DA, Pfeiffer C, Pelaz B, Parak WJ. Characterization of hydrophilic coated gold nanoparticles via capillary electrophoresis and Taylor dispersion analysis. Part II: Determination of the hydrodynamic radius distribution – Comparison with asymmetric flow field-flow fractionation. J Colloid Interface Sci 2015;457:131–40.
[15] Kankala RK, Han Y-H, Na J, Lee C-H, Sun Z, Wang S-B, et al. Nanoarchitectured Structure and Surface Biofunctionality of Mesoporous Silica Nanoparticles. Adv Mater 2020;32:1907035.
[16] Kumar H, Venkatesh N, Bhowmik H, Kuila A. Metallic Nanoparticle: A Review. Biomed J Sci Tech Res 2018;4:3765–75.
[17] Evans ER, Bugga P, Asthana V, Drezek R. Metallic nanoparticles for cancer immunotherapy. Mater Today 2018;21:673–85.
[18] Jamkhande PG, Ghule NW, Bamer AH, Kalaskar MG. Metal nanoparticles synthesis: An overview on methods of preparation, advantages and disadvantages, and applications. J Drug Deliv Sci Technol 2019;53:101174.
[19] Taylor GI. Dispersion of soluble matter in solvent flowing slowly through a tube. Proc R Soc Lond Ser Math Phys Sci 1953;219:186–203.
[20] Adamo G, Campora S, Ghersi G. Chapter 3 - Functionalization of nanoparticles in specific targeting and mechanism release. In: Ficai D, Grumezescu AM, editors. Nanostructures Nov. Ther., Elsevier; 2017, p. 57–80.
[21] Moser MR, Baker CA. Taylor dispersion analysis in fused silica capillaries: a tutorial review. Anal Methods 2021;13:2357–73.
[22] Labied L, Rocchi P, Doussineau T, Randon J, Tillement O, Lux F, et al. Taylor Dispersion Analysis Coupled to Inductively Coupled Plasma-Mass Spectrometry for Ultrasmall Nanoparticle Size Measurement: From Drug Product to Biological Media Studies. Anal Chem 2021;93:1254–9.
[23] d'Orlyé F, Varenne A, Gareil P. Determination of nanoparticle diffusion coefficients by Taylor dispersion analysis using a capillary electrophoresis instrument. J Chromatogr A 2008;1204:226–32.
[24] Taladriz-Blanco P, Rothen-Rutishauser B, Petri-Fink A, Balog S. Resolution Limit of Taylor Dispersion: An Exact Theoretical Study. Anal Chem 2020;92:561–6.
[25] Ramírez-García G, Oluwole DO, Nxele SR, d'Orlyé F, Nyokong T, Bedioui F, et al. Characterization of phthalocyanine functionalized quantum dots by dynamic light scattering, laser Doppler, and capillary electrophoresis. Anal Bioanal Chem 2017;409:1707–15.
[26] Pyell U, Jalil AH, Pfeiffer C, Pelaz B, Parak WJ. Characterization of gold nanoparticles with different hydrophilic coatings via capillary electrophoresis and Taylor dispersion analysis. Part I: Determination of the zeta potential employing a modified analytic approximation. J Colloid Interface Sci 2015;450:288–300.
[27] Girardot M, d'Orlyé F, Varenne A. Electrokinetic characterization of superparamagnetic nanoparticle–aptamer conjugates: design of new highly

specific probes for miniaturized molecular diagnostics. Anal Bioanal Chem 2014;406:1089–98.
[28] Höldrich M, Liu S, Epe M, Lämmerhofer M. Taylor dispersion analysis, resonant mass measurement and bioactivity of pepsin-coated gold nanoparticles. Talanta 2017;167:67–74.
[29] Ibrahim A, Ohshima H, Allison SA, Cottet H. Determination of effective charge of small ions, polyelectrolytes and nanoparticles by capillary electrophoresis. J Chromatogr A 2012;1247:154–64.
[30] Labied L, Rocchi P, Doussineau T, Randon J, Tillement O, Cottet H, et al. Biodegradation of metal-based ultra-small nanoparticles: A combined approach using TDA-ICP-MS and CE-ICP-MS. Anal Chim Acta 2021;1185:339081.
[31] Degasperi A, Labied L, Farre C, Moreau E, Martini M, Chaix C, et al. Probing the protein corona of gold/silica nanoparticles by Taylor dispersion analysis-ICP-MS. Talanta 2022;243:123386.
[32] Bello MS, Rezzonico R, Righetti PG. Use of Taylor-Aris Dispersion for Measurement of a Solute Diffusion Coefficient in Thin Capillaries. Science 1994;266:773–6.
[33] Sharma U, Gleason NJ, Carbeck JD. Diffusivity of Solutes Measured in Glass Capillaries Using Taylor's Analysis of Dispersion and a Commercial CE Instrument. Anal Chem 2005;77:806–13.
[34] Belongia BM, Baygents JC. Measurements on the Diffusion Coefficient of Colloidal Particles by Taylor–Aris Dispersion. J Colloid Interface Sci 1997;195:19–31.
[35] Cottet H, Biron J-P, Martin M. Taylor Dispersion Analysis of Mixtures. Anal Chem 2007;79:9066–73.
[36] Pecora R. Dynamic Light Scattering Measurement of Nanometer Particles in Liquids. J Nanoparticle Res 2000;2:123–31.
[37] Touré M, Chamieh J, Arrachart G, Pellet-Rostaing S, Cottet H, Duhamet J. Mass transfer efficiency in rare earth extraction using a hollow fiber pertraction device. Sep Purif Technol 2020;251:117330.
[38] Chamieh J, Leclercq L, Martin M, Slaoui S, Jensen H, Østergaard J, et al. Limits in Size of Taylor Dispersion Analysis: Representation of the Different Hydrodynamic Regimes and Application to the Size-Characterization of Cubosomes. Anal Chem 2017;89:13487–93.
[39] Cottet H, Biron J-P, Martin M. On the optimization of operating conditions for Taylor dispersion analysis of mixtures. Analyst 2014;139:3552–62.
[40] Chapman AJS, Goodall DM. A novel approach to measurement of hydrodynamic radius for a standard protein using UV area imaging detection. Chromatogr Today n.d.
[41] Chamieh J, Cottet H. Comparison of single and double detection points Taylor Dispersion Analysis for monodisperse and polydisperse samples. J Chromatogr A 2012;1241:123–7.
[42] Chamieh J, Oukacine F, Cottet H. Taylor dispersion analysis with two detection points on a commercial capillary electrophoresis apparatus. J Chromatogr A 2012;1235:174–7.
[43] Scotti A, Liu W, Hyatt JS, Herman ES, Choi HS, Kim JW, et al. The CONTIN algorithm and its application to determine the size distribution of microgel suspensions. J Chem Phys 2015;142:234905.